Effects of effective attractive multi-body interaction on quantum phase and transport dynamics of a strongly correlated bosonic gas across the superfluid to Mott insulator transition*

Sun Jian-Fang(孙剑芳)[a)b)], Cui Guo-Dong(崔国栋)[a)b)], Jiang Bo-Nan(姜伯楠)[a)b)], Qian Jun(钱 军)[a)†], and Wang Yu-Zhu(王育竹)[a)‡]

[a)] *Key Laboratory for Quantum Optics, Center for Cold Atom Physics, Shanghai Institute of Optics and Fine Mechanics, Chinese Academy of Sciences, Shanghai* 201800, *China*

[b)] *University of Chinese Academy of Sciences, Beijing* 100049, *China*

(Received 21 June 2013; revised manuscript received 14 August 2013)

We theoretically investigate quantum phases and transport dynamics of ultracold atoms trapped in an optical lattice in the presence of effective multi-body interaction. When a harmonic external potential is added, several interesting phenomena are revealed, such as the broadening and the emergence of a central insulator plateau and the phase transition between superfluid and Mott insulator phase. We also study the transport of the system which runs across the superfluid–insulator transition after ramping up the lattice, and predict a slower relaxation which is attributed to the influence of the multi-body interaction on the mass transport.

Keywords: Bose–Hubbard model, three-body interaction

PACS: 03.75.Lm, 03.75.Kk, 67.85.–d, 05.60.Gg **DOI:** 10.1088/1674-1056/22/11/110307

1. Introduction

Ultracold atoms in an optical lattice (OL) offer a unique setting for quantum simulation of interacting many-body systems due to its outstanding controllability of lattice parameters and atomic interaction strength.[1] As an important milestone, the observation of superfluid (SF) to Mott insulator (MI) transition[2,3] has stimulated the exploration of a variety of novel quantum phases.[4–8] Conventionally, only the ground band has to be considered in a standard Bose–Hubbard model (BHM), however, the multi-band effect has been measured in quantum phase revival spectroscopy[9,10] and has also been demonstrated to play an essential role in photon-assisted tunneling.[11] In fact, in a deep lattice, the single-band assumption should be checked carefully and the virtual transitions to higher excited bands should be renormalized to effective multi-body interactions of atoms in the lowest band.[12] It has been found that the visibility of interference fringes depend on both two-, three-, and multi-body energy scales in the collapse and revival dynamics. Such an unusual multi-body effect has also been theoretically studied for the repulsive multi-body interaction.[13–16] Novel quantum phases have been revealed, such as the extension of the insulating lobes in the optical lattice and the superlattice, the existence of a fixed point in the three-dimensional phase space, and the phase diagram of a dipolar Bose–Einstein condensation in an optical lattice with both two- and three-body repulsive interactions. In addition, extensive studies have focused on the non-equilibrium dynamics of a strongly correlated system with trapped atoms in OLs,[17–21] especially the whole process of the SF–MI transition.[22–26] Experimentally, the lattice depth can be adjusted by tuning the laser intensity of the lattice, and the mutual atom interaction can be controlled by using the Feshbach resonance technique.[27] In particular, different timescales have been found by several groups, which further shows the local and global transport within different lattice ramp time.[23,24]

In this work, instead of the repulsive three-body interaction, an attractive three-body interaction is chosen according to the experimental measurement.[9–11] We study the effects of the attractive three-body interaction on the phases of the bosonic system at equilibrium and explore the non-equilibrium dynamics across the SF–MI transition. This paper is arranged as follows. In Section 2, we briefly introduce the Gutzwiller mean-field theory to deal with our modified Hamiltonian, and present the phase diagram of the ground state. Our results differ from those in Refs. [13] and [14] where the three-body interaction is repulsive. In Section 3, we show several intriguing phenomena for a trapped lattice gas, such as the broadening and the emergence of a central MI plateau and the phase transition between SF and MI. In addition, we also demonstrate a slower relaxation of the system when it experi-

*Project supported by the National Basic Research Program of China (Grant No. 2011CB921504) and the National Natural Science Foundation of China (Grant No. 11104292).

†Corresponding author. E-mail: jqian@siom.ac.cn

‡Corresponding author. E-mail: yzwang@mail.shcnc.ac.cn

© 2013 Chinese Physical Society and IOP Publishing Ltd

ences the crossover from the SF phase to the insulating phase during the evolution of 400 ms.

2. Theoretical model and phase diagram

We consider a single-component bosonic gas loaded into a 2D optical lattice, which is described by the renormalized single-band BHM including an on-site binary interaction and an effective three-body interaction

$$\hat{H} = -J\sum_{\langle i,j\rangle}(\hat{b}_i^\dagger\hat{b}_j+\text{h.c.})+\frac{U_2}{2}\sum_i\hat{n}_i(\hat{n}_i-1) + \frac{U_3}{6}\sum_i\hat{n}_i(\hat{n}_i-1)(\hat{n}_i-2)-\mu\sum_i\hat{n}_i, \quad (1)$$

where $\hat{b}_i$ ($\hat{b}_i^\dagger$) is the bosonic annihilation (creation) operator on site i, U_2, and U_3 are the binary and three-body interaction strengths, respectively, J is the tunneling matrix element, and μ is the chemical potential introduced to conserve the number of atoms in the grand-canonical ensemble. For simplicity, we only include the attractive three-body interaction term because the higher-order effect is usually very small.[9,11] By applying Gutzwiller ansatz $\hat{b}_j=\psi+\delta\hat{b}_j$ ($\psi=\langle\hat{b}_j\rangle$ is an order parameter), the above BHM Hamiltonian can be further simplified to a site-decoupled Hamiltonian

$$\hat{H}^{\text{eff}}=\sum_i\hat{H}_i^{\text{eff}},$$

with

$$\hat{H}_i^{\text{eff}} = -zJ(\hat{b}_i^\dagger+\hat{b}_i)\psi+zJ\psi^2+\frac{1}{2}U_2\hat{n}_i(\hat{n}_i-1) + \frac{1}{6}U_3\hat{n}_i(\hat{n}_i-1)(\hat{n}_i-2)-\mu\hat{n}_i, \quad (2)$$

where $z=4$ for the 2D case. Then we apply the perturbation theory to obtain the ground state and the phase diagram. The effective Hamiltonian (2) can be written as

$$\hat{H}_i^{\text{eff}}/zJ=\hat{H}_i^{(0)}-(\hat{b}_i^\dagger+\hat{b}_i)\psi, \quad (3)$$

which includes the unperturbed Hamiltonian $\hat{H}_i^{(0)}=\psi^2+\frac{1}{2}\bar{U}_2\hat{n}_i(\hat{n}_i-1)+\frac{1}{6}\bar{U}_3\hat{n}_i(\hat{n}_i-1)(\hat{n}_i-2)-\bar{\mu}\hat{n}_i$ and the hopping term. All parameters $(\bar{U}_2,\bar{U}_3,\bar{\mu})$ are scaled by zJ. In the absence of tunneling, the unperturbed ground state is a local Fock state $|n\rangle$ with an integer filling. The corresponding energy is $E^{(0)}=\frac{1}{2}\bar{U}_2n(n-1)+\frac{1}{6}\bar{U}_3n(n-1)(n-2)-\bar{\mu}n$. The second-order perturbation in energy gives

$$E^{(2)} = \frac{n+1}{-\bar{U}_2n-\frac{1}{2}\bar{U}_3n(n-1)+\bar{\mu}} + \frac{n}{\bar{U}_2(n-1)+\frac{1}{2}\bar{U}_3(n-1)(n-2)-\bar{\mu}}. \quad (4)$$

From the phase boundary relation $E^{(2)}+1=0$, we can obtain the upper and lower branches of the MI lobe with filling n

$$\bar{\mu}_\pm(n) = \frac{1}{2}\left[\bar{U}_2(2n-1)+\gamma\bar{U}_2(n-1)^2-1\right]\pm\frac{1}{2}\sqrt{\bar{U}_2^2\left[1+\gamma(n-1)\right]^2-2(2n+1)\left[1+\gamma(n-1)\right]\bar{U}_2+1}, \quad (5)$$

here we define a parameter $\gamma=U_3/U_2$, which characterizes the strength of the multi-body interaction.

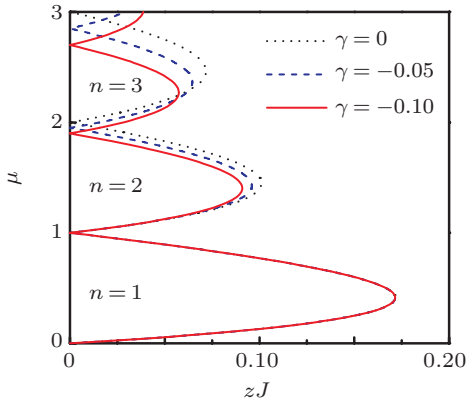


Fig. 1. (color online) Phase diagram of the modified BHM (1) for $\gamma=0$, -0.05, -0.1.

Now the phase boundaries of the non-standard BHM discussed here can be derived from Eq. (5), the corresponding phase diagram is depicted in Fig. 1. It is quite clear that the presence of the effective multi-body interaction has a remarkable influence on the phases of the ultracold atoms in OLs. It is no surprise that, at unity filling, the phase boundary agrees perfectly with the standard BHM no matter whether the three-body interaction exists or not. In fact, in this situation, the sites are singly occupied and the interaction almost does not work. When we look at the lobes filled with more atoms, however, the phase boundary shows an amazing change compared to the results of $\gamma=0$. In the case of repulsive three-body interaction, the insulating lobes with filling $n>1$ become larger and wider, while, in this work, the situation changes as follows.[13,14] First, we find that the critical value $(zJ/U_2)_c$, where the system experiences the SF–MI crossover, has a strong dependence on γ. In our work, for a fixed total number of atoms in the optical lattice, $(zJ/U_2)_c$ decreases with increasing $|\gamma|$. We realize that the multi-body correction to the on-site energy lowers the total interaction energy because of the attractive effective three-body interaction ($\gamma<0$). It means that less power of the lattice laser is required to ramp the lattice depth down and to release the frozen atoms at each site in the MI zone. Moreover, the critical point of the SF–MI transition is also related

to the filling n. To understand this quantitatively, we solve the equation $\bar{\mu}_+(n) = \bar{\mu}_-(n)$ and give the expression of the critical value for the SF–MI transition

$$(zJ/U_2)_c = [1+\gamma(n-1)] \Big/ \left[(2n+1)+\sqrt{(2n+1)^2-1}\right]. \quad (6)$$

It is obvious that the parameter γ appears in the numerator of Eq. (6) associated with the filling n. This term distinguishes the standard BHM from the present model. Given a negative γ and for a filling more than unity, one can easily find that $(zJ/U_2)_c$ becomes smaller for a larger n, so the critical point moves leftwards in Fig. 1.

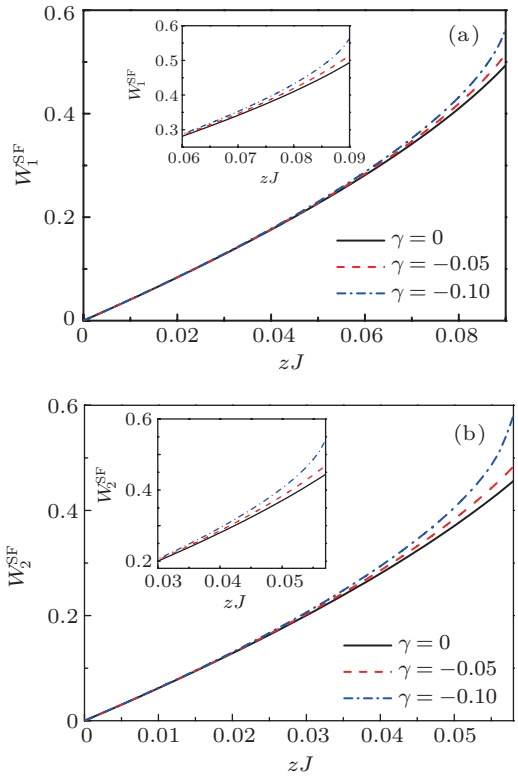


Fig. 2. (color online) Width of SF phase between neighbor MI plateaus: (a) W_1^{SF}, (b) W_2^{SF}.

In addition to the shift of the transition point, we also find that the width of the MI lobes at a fixed (zJ/U) is closely related to the effective three-body interaction. In fact, this width is related to the shell structure of the inhomogeneous lattice bosonic gas. Then we have the following relation for the MI plateau with n atoms at each site

$$(n-1)[1+\gamma/2(n-2)]\bar{U}_2 < \bar{\mu} < n[1+\gamma/2(n-1)]\bar{U}_2. \quad (7)$$

Similar to Eq. (6), the effective three-body interaction contributes additional terms that involve γ and n, resulting in the shrinkage of the lobes.

For an inhomogeneous lattice gas in the MI regime, one can clearly observe cake-like shells, which are separated by the SF rings.[4,5] We can define the width of an SF zone between neighbor MI plateaus as $W_n^{SF} = \mu_-(n+1) - \mu_+(n)$, which corresponds to the distance between the lower boundary of the MI lobe with $n+1$ atoms and the upper boundary of the MI lobe with the filling factor n in the phase diagram. From Eq. (5), we can obtain W_n^{SF} varying with the tunneling J, which is plotted in Fig. 2. Once the lattice is ramped down, more frozen atoms are released from the MI regions and the SF rings become wider and wider. It is apparent that the width is hardly dependent on γ when the lattice is very deep (very small J). However, it will curve up away from the black solid line ($\gamma = 0$) for a swallow lattice, which means that a larger attractive multi-body interaction results in a larger value of W_n^{SF}. Given the chemical potential $\mu = 2.2U_2$, each site is occupied by three atoms in the innermost zone. From the phase diagram, one can observe an expansion of the central MI plateau and a narrowing MI shell of $n = 2$, while the shell with unity filling is unchanged. Hence, W_1^{SF} grows gradually. Here we point out that the shrinkage of the insulator plateau ($n = 2$) predominates over the expansion of the $n = 3$ MI plateau, so the value of W_2^{SF} becomes larger.

3. Numerical results and discussion

In the above discussion, we analyzed the phase diagram and shell structure of an inhomogeneous lattice gas in detail. In this section, we further calculate the ground state and time evolution of the system using a time-dependent Gutzwiller ansatz $|\Phi_G\rangle = \Pi_i|\phi_i\rangle$, where $|\phi_i\rangle = \sum_{n=0} c_n^{(i)}(t)|n\rangle_i$ and $|n\rangle_i$ is the n-atom Fock state on site i. Furthermore, the effect of the harmonic trap potential is included in a local density approximation with a quadratically changing chemical potential $\mu_i = \mu - V_{ex}(i)$. Then we arrive at the inhomogeneous version of Eq. (2)

$$\begin{aligned}\hat{H}_i^{eff} &= -zJ(\hat{b}_i^\dagger\beta_j + \beta_j^*\hat{b}_i) + zJ|\beta_j|^2 + \frac{1}{2}U_2\hat{n}_i(\hat{n}_i-1) \\ &\quad + \frac{1}{6}U_3\hat{n}_i(\hat{n}_i-1)(\hat{n}_i-2) - \mu_i\hat{n}_i, \end{aligned} \quad (8)$$

where $\beta_j = 1/z\sum_{\langle j\rangle}\langle\hat{a}_j\rangle$ is the sum over j including all the nearest neighbor sites. Using the above site-decoupled Hamiltonian, we update the wavefunction by iteratively performing the real-time Crank–Nicolson (CN) algorithm[28,29] between time steps

$$|\phi_i^{(n+1)}\rangle = \frac{1-i\frac{1}{2}\Delta t\hat{H}_i^{eff}(\beta_j^{(n)})}{1+i\frac{1}{2}\Delta t\hat{H}_i^{eff}(\beta_j^{(n)})}|\phi_i^{(n)}\rangle, \quad (9)$$

here n and Δt denote the iteration number and the time step size, respectively. Similarly, the imaginary-time CN algorithm is used to solve the ground state wavefunction.[30] In addition, in order to conserve the total atom number and energy, we use sequential site updates in the time evolution.[15,24]

Now we begin to investigate the effects of the multi-body interaction on the quantum phases of the strongly-correlated

system with ultracold atoms in optical lattices. For clarity, we consider several special cases in the phase diagram and find remarkable changes of the density profiles due to the effective multi-body interaction. The three-body interaction strength $U_3 = -0.1U_2$, i.e., $\gamma = -0.1$, is chosen.[9,11] Because of the circular symmetry, we only provide the profiles of ^{87}Rb atoms in the $y = 0$ plane. In the first case (Fig. 3(a)), the central region transforms from an MI phase with two atoms at each site to an SF phase when γ becomes nonzero; this means that the effective three-body interaction drastically alters the phase of the strongly correlated system. The corresponding phase (zJ, μ) highlighted by the red star in Fig. 3(e) is located in the MI region when $\gamma = 0$, however, it becomes a superfluid phase when $\gamma = -0.1$, because the $n = 2$ lobe shrinks and the phase boundary moves leftwards in this case.

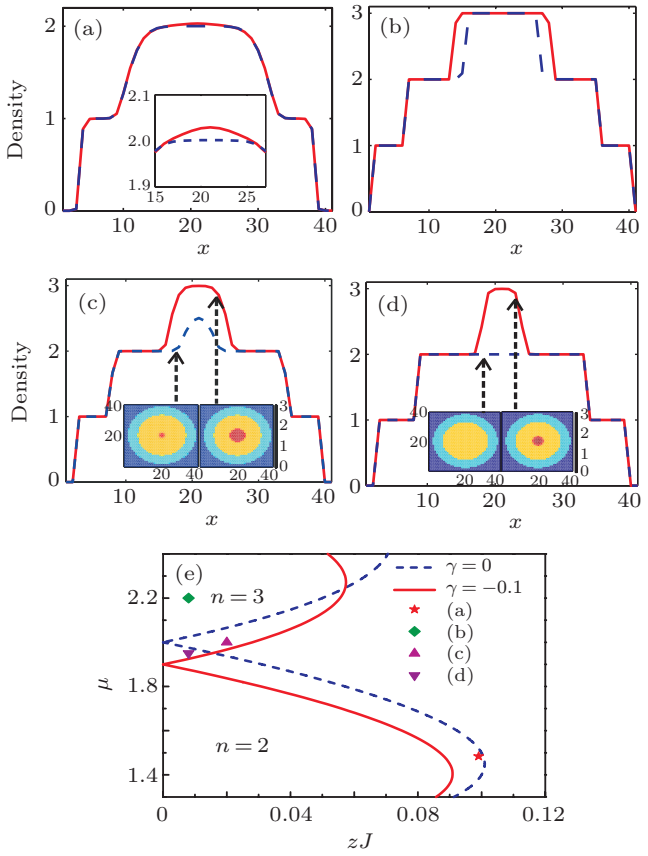


Fig. 3. (color online) Atomic density distributions in the $y = 0$ plane in the absence ($\gamma = 0$, blue dashed line) and the presence ($\gamma = -0.1$, red solid line) of the effective three-body interaction. The values of (zJ, μ, V_0) are (a) (0.1, 1.5, 15), (b) (0.008, 2.2, 26), (c) (0.02, 2, 22), and (d) (0.008, 1.95, 26). Here, V_0 is the trap depth scaled by the recoil energy of the lattice photons. Other parameters are in units of U_2. The cases are also highlighted in the phase diagram (e). The insets in panels (c) and (d) are the density distributions in the x–y plane.

One can also observe another interesting result in Fig. 3(b), which corresponds to the phase marked by the blue diamond in Fig. 3(e). The central insulating terrace expands outward and occupies a larger region when γ is nonzero. In this situation, the phase boundary between the MI plateaus with $n = 2, 3$ atoms and the sandwiched SF region move downward simultaneously in the presence of the effective multi-body interaction, which leads to the expansion of the innermost insulating plateau. Because the three-body interaction shrinks the MI regions except for the $n = 1$ MI shell, the width of the MI shell with double occupancy reduces and the shell occupies fewer lattice sites; meanwhile, the $n = 1$ MI shell does not change and the range of the $n = 3$ MI plateau becomes large.

Contrary to the transformation from MI to SF phase shown in Fig. 3(a), we demonstrate an intriguing opposite effect of the effective three-body interaction in Fig. 3(c). Now the mobile atoms in the central zone are frozen and a new insulating plateau appears and replaces the original SF core. When only the binary interaction is present, the state at equilibrium in the center is located in the SF phase marked by the pink up-triangle in Fig. 3(e). Once the three-body interaction is added, the phase boundary goes down and the state should enter the insulating lobe, which can be easily discriminated in an *in-situ* imaging detection[22,31–33] (see the inset in Fig. 3(c)). Furthermore, one of the most surprising changes of the quantum phase is shown in Fig. 3(d). The multi-body interaction leads to the unexpected emergence of a new insulating plateau with filling $n = 3$ in the background of the original MI plateau. It is very clear when we compare the density profiles (the inset in Fig. 3(d)) in the presence and in the absence of U_3. The notable difference can be explained by the phase diagram, in which both the $n = 2$ and $n = 3$ lobes move downwards together. Thus the corresponding point in the phase diagram exits the $n = 2$ lobe and enters into the $n = 3$ lobe.

From the above discussion, we can conclude that the effective multi-body interaction has a remarkable influence on the phase of the strongly correlated atomic system at equilibrium. Next we explore several different scenarios to fully reveal the response of the system in the presence of the effective multi-body interaction. Specifically, we study the non-equilibrium dynamics of the inhomogeneous system while linearly increasing the lattice depth from $V_\mathrm{i} = 11$ Er to $V_\mathrm{f} = 17$ Er within variable time τ_r. The chemical potential μ is chosen such that the atom number on each site at the final equilibrium state in the central zone is close to two when only the binary interaction is present. It is obvious that the situation discussed here is quite different from that in Ref. [24] because of the high central occupation at the initial state. For simplicity, we assume γ to be constant during the evolution, which is approximatively valid.[9] By varying the three-body interaction coefficient γ, we obtain the final density profiles after ramp time $\tau_\mathrm{r} = 120 \times 2\pi/U_2^{\mathrm{ini}} \sim 400$ ms (see Figs. 4(a)–4(c)), here U_2^{ini} is the binary interaction strength at the beginning. For comparison, we also show the initial SF state and the final insulating state at equilibrium in Figs. 4(a)–4(c).

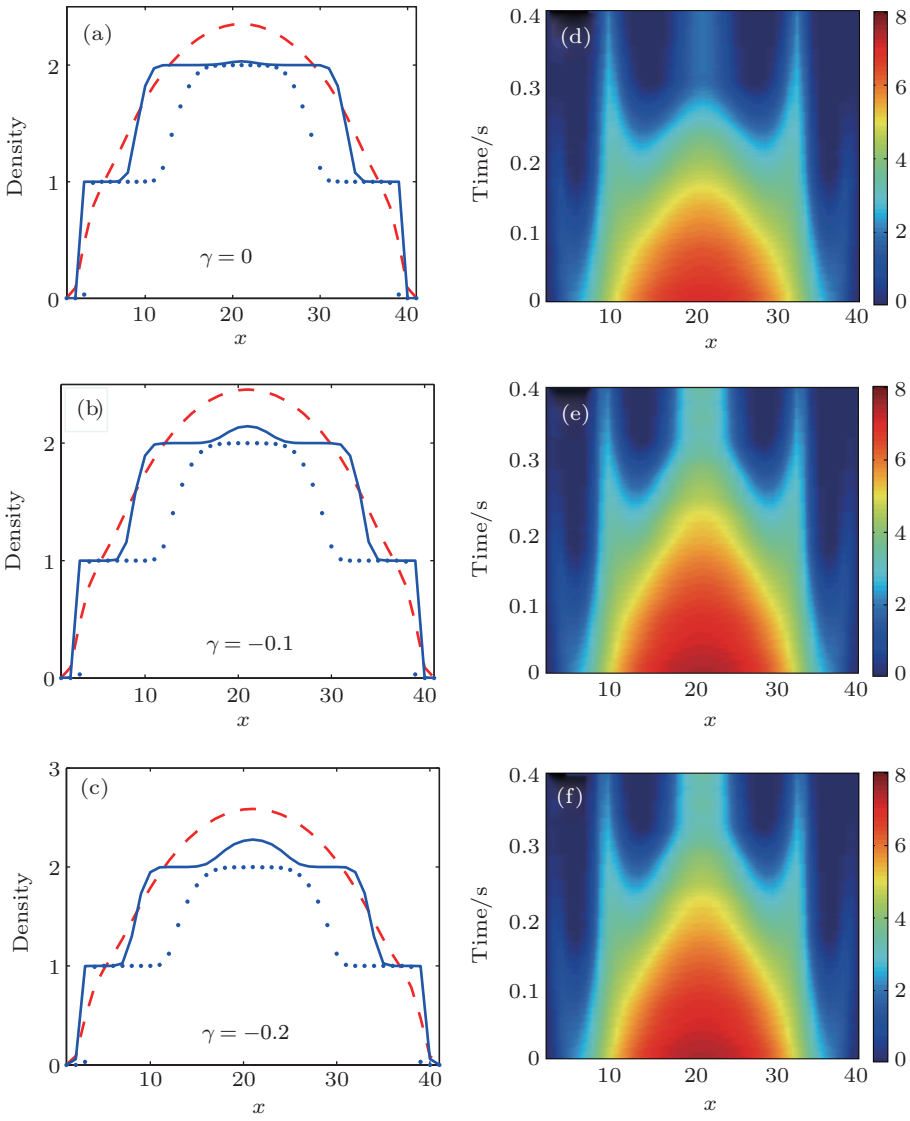


Fig. 4. (color online) Density profiles of the trapped gas (left panels) and time evolution of the coherence (right panels) at different three-body interaction strengths: (a) and (d) $\gamma = 0$, (b) and (e) $\gamma = -0.1$, (c) and (f) $\gamma = -0.2$. The dashed (red) and dotted (blue) lines denote the initial and the final states at equilibrium associated with the lattice depths $V_i = 11$ Er and $V_f = 17$ Er, respectively. The solid (blue) line is the final density profile after ramp time $\tau_r = 120 \times 2\pi/U_2 \sim 400$ ms. The color from blue to red represents the crossover from the Mott-insulator regions to the SF regions with large coherence.

For $\gamma = 0$ (Fig. 4(a)), although the system does not arrive at the equilibrium, the atomic distribution in the central zone is close to that of the final state at equilibrium. In this sense, when we only pay special attention to the evolution process of the system in the central region of the trap, a local equilibration has been reached in this situation. As shown in Fig. 4(b), when a small three-body interaction ($\gamma = -0.1$) is introduced, the final profile deviates markedly from that of the final state at equilibrium in the innermost zone where an SF phase emerges. With the increasing three-body interaction strength ($\gamma = -0.2$), the range of the central SF phase obviously extends outward, which leads to a highly remarkable deviation between the final equilibrium and non-equilibrium states. It has been demonstrated definitively in these results that the attractive three-body interaction slows down the relaxation of the system towards the equilibrium. To better understand the time evolution of the many-body ensemble, we numerically calculate the coherence $\mathcal{C}_i = \langle a_i \rangle \sum_j \langle a_j^* \rangle$ [24] when the lattice is ramped up gradually in 400 ms and the system evolves from a given SF phase with high coherence as depicted in Figs. 4(d)–4(f). Similarly, we also provide the result when the multi-body interaction is lacking in the whole process (see Fig. 4(d)). In this situation, a large insulating region appears after about 200 ms. At last, an MI plateau with two atoms at each site forms in the center, which is also surrounded with a remaining SF ring. However, the situation is quite different when the multi-body interaction works, just like the cases in Figs. 4(e) and 4(f). The crucial discovery is that an SF core remains and is accompanied by a growing insulating shell. Furthermore, one can observe that the SF core covers quite a few

sites especially when U_3 is enhanced. From these results, one can intuitively realize that the key to the observation of slow relaxation in our system is the presence of the renormalized multi-body interaction. In fact, it has been found that the mass transport between SF regions plays an increasingly important role in non-equilibrium dynamics of the ensemble in the situation when only the binary atomic interaction is involved.[24] It is in favor of global equilibration that insulating regions appear as early in the procedure of the transport as possible, because they can block the particle flow from one SF ring to another. It is quite clear from the comparison between the moments of the MI shell that happened near the center in Figs. 4(d)–4(f) that the effective multi-body interaction really postpones the appearance of the insulating region. For example, the MI shell begins to grow until about 250 ms when $\gamma = -0.2$ (Fig. 4(f)) rather than 200 ms in Fig. 4(d). Moreover, the wider the MI regions are, the more remarkable the blockade is. In our system, a large attractive three-body interaction decreases greatly the total interaction energy and makes it harder to turn the central zone into a complete insulating phase compared to the case with only the binary interaction. Besides, more atoms are located in the center of the trap and will strikingly strengthen the falling tendency of the interaction energy. That is the true answer why such an SF core can occupy much space in the situation of $\gamma = -0.2$. Considering the aforementioned discoveries of the delayed MI shell and the wide SF core, one can easily conclude that the mass transport between different SF regions cannot be readily blocked especially when γ becomes significant.

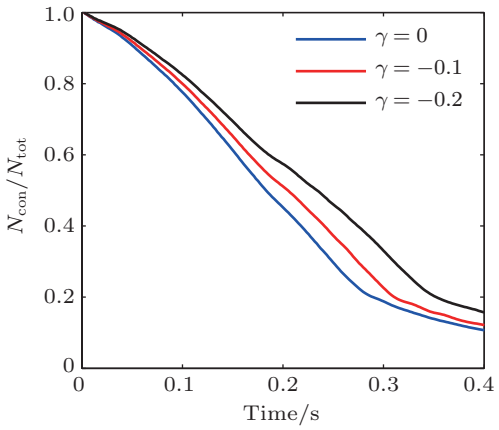


Fig. 5. (color online) Time evolution of condensate ratio.

We further calculate the macroscopic quantities, total atom number $N_{\rm tot}(t) = \sum_{\mathcal{Z}} n_{i,j}(t)$ and condensate fraction $N_{\rm con}(t) = \sum_{\mathcal{Z}} |\langle \hat{b}_{i,j}(t) \rangle|^2$,[34] within the innermost zone $\mathcal{Z}$ of 20×20 sites. Here we ignore the outmost MI regions only singly occupied because the $n = 1$ MI shell has a negligible change due to the presence of the multi-body interaction. The condensate ratio $N_{\rm con}/N_{\rm tot}$ as a function of time is shown in Fig. 5, from which one can see that the condensate ratio decreases with time. Here the rapid depletion of the condensate fraction indicates the growth of the MI regions. We have observed a slower reduction of $N_{\rm con}/N_{\rm tot}$ in the cases of $\gamma \neq 0$ and found that the final value of the depleted condensate is strongly dependent on γ. Remarkably, in an ensemble with large γ, the SF remains in the central region.

4. Conclusion

In summary, we have explored novel quantum phases and mass transport of ultracold bosons in an optical lattice and the influence of the renormalized multi-body interaction. Several intriguing phenomena, including an expanding MI zone and the emergence of a new MI terrace, have been demonstrated in the mean-field calculations. We also induced quantum quench by lifting the lattice depth and investigated the dynamical response of the system. Compared to the situation in the absence of the multi-body interaction, the relaxation towards equilibrium becomes slower when the three-body interaction cannot be ignored. Since the ingredients mentioned above, such as the effective multi-body interaction and the related detection techniques, have been realized experimentally, our results are expected to be relevant to experimental situations realizable in the near future. Other issues closely related to non-equilibrium dynamics beyond single-band BHM as we have done in this work are also expected to be raised and resolved.

References

[1] Bloch I, Dalibard J and Zwerger W 2008 *Rev. Mod. Phys.* **80** 885
[2] Jaksch D, Bruder C, Cirac J I, Gardiner C W and Zoller P 1998 *Phys. Rev. Lett.* **81** 3108
[3] Greiner M, Mandel O, Esslinger T, Hänsch T W and Bloch I 2002 *Nature* **415** 39
[4] Campbell G K, Mun J, Boyd M, Medley P, Leanhardt A E, Marcassa L G, Pritchard D E and Ketterle W 2006 *Science* **313** 649
[5] Fölling S, Widera A, Müller T, Gerbier F and Bloch I 2006 *Phys. Rev. Lett.* **97** 060403
[6] Wang Y M and Liang J Q 2012 *Chin. Phys. B* **21** 060305
[7] Zhu R 2007 *Chin. Phys. Lett.* **24** 797
[8] Tie L and Xue J K 2011 *Chin. Phys. B* **20** 120311
[9] Will S, Best T, Schneider U, Hackermüller L, Lühmann D S and Bloch I 2010 *Nature* **465** 197
[10] Will S, Best T, Braun S, Schneider U and Bloch I 2011 *Phys. Rev. Lett.* **106** 115305
[11] Ma R C, Tai M E, Preiss P M, Bakr W S, Simon J and Greiner M 2011 *Phys. Rev. Lett.* **107** 095301
[12] Johnson P R, Tiesinga E, Porto J V and Williams C J 2009 *New J. Phys.* **11** 093022
[13] Singh M, Dhar A, Mishra T, Pai R V and Das B P 2012 *Phys. Rev. A* **85** 051604
[14] Chen B L, Huang X B, Kou S P and Zhang Y B 2008 *Phys. Rev. A* **78** 043603
[15] Zhou K Z, Liang Z X and Zhang Z D 2010 *Phys. Rev. A* **82** 013634
[16] Silva-Valencia J and Souza A M C 2012 *Eur. Phys. J. B* **85** 161
[17] Kinoshita T, Wenger T and Weiss D S 2006 *Nature* **440** 900
[18] Hackermüller L, Schneider U, Moreno-Cardoner M, Kitagawa T, Best T, Will S, Demler E, Altman E, Bloch I and Paredes B 2010 *Science* **327** 1621

[19] Cao C, Elliott E, Joseph J, Wu H, Petricka J, Schäfer T and Thomas J E 2011 *Science* **331** 58

[20] Gerbier F, Trotzky S, Fölling S, Schnorrberger U, Thompson J D, Widera A, Bloch I, Pollet L, Troyer M, Capogrosso-Sansone B, Prokofév N V and Svistunov B V 2008 *Phys. Rev. Lett.* **101** 155303

[21] Rohzheimer J P, Schreiber M, Braun S, Hodgman S S, Langer S, McCulloch I P, Heidrich-Meisner F, Bloch I and Schneider U 2013 *Phys. Rev. Lett.* **110** 205301

[22] Bakr W S, Peng A, Tai M E, Ma R, Simon J, Gillen J I, Fölling S, Pollet L and Greiner M 2010 *Science* **329** 547

[23] Hung C L, Zhang X B, Gemelke N and Chin C 2010 *Phys. Rev. Lett.* **104** 160403

[24] Natu S S, Hazzard K R A and Mueller E J 2011 *Phys. Rev. Lett.* **106** 125301

[25] Cheneau M, Barmettler P, Poletti D, Endres M, Schauß P, Fukuhara T, Gross C, Bloch I, Kollath C and Kuhr S 2012 *Nature* **481** 484

[26] Endres M, Cheneau M, Fukuhara T, Weitenberg C, Schauß P, Gross C, Mazza L, Bañuls M C, Pollet L, Bloch I and Kuhr S 2011 *Science* **334** 200

[27] Chin C, Grimm R, Julienne P and Tiesinga E 2010 *Rev. Mod. Phys.* **82** 1225

[28] Press W H, Teukolsky S A, Vetterling W T and Flannery B P 1992 *Numerical Recipes in C* (2nd edn) (Cambridge: Cambridge University Press)

[29] Javanainen J and Ivanov M Y 1999 *Phys. Rev. A* **60** 2351

[30] Yamashita M and Jack M W 2009 *Phys. Rev. A* **79** 023609

[31] Bakr W S, Gillen J I, Peng A, Fölling S and Greiner M 2009 *Nature* **462** 74

[32] Sherson J F, Weitenberg C, Endres M, Cheneau M, Bloch I and Kuhr S 2010 *Nature* **467** 68

[33] Endres M, Cheneau M, Fukuhara T, Weitenberg C, Schauß P, Gross C, Mazza L, Bañuls M C, Pollet L, Bloch I and Kuhr S 2013 arXiv:1303.5652v1

[34] Rapp Á 2013 *Phys. Rev. A* **87** 043611